

Research of radiation characteristics of high-power CO₂-laser with the controlled pumping pulse

V.V. Osipov, V.V. Lisenkov, N.V. Gavrilov,
O.A. Bureev, V.A. Shitov, and A.A. Malyshkin

*Institute of Electrophysics,
Ural Branch of the Russian Academy of Sciences, Ekaterinburg*

Received November 15, 2005

Results of studies of high-power pulse-periodic electroionization CO₂-laser radiation characteristics are presented. To generate the e-beam, controlling a gas discharge, an accelerator with plasma emitter of electrons based on the low-pressure glow discharge with a hollow cathode and anode was used, which allowed a sharp increase of the e-beam current and control for its duration. The laser pulse duration varied in a range 300–1200 μ s. An energy of 200 J and an efficiency of 18% were obtained. Optimal conditions for pumping, generation, and focusing laser radiation were determined.

Introduction

Studies of semi-self-maintained volume discharge conducted under the direction of G.A. Mesyats,¹ and the discovery by Patel of generation at CO₂ molecule vibration transitions,² have formed grounds for creation of high-power high-pressure CO₂ lasers. The active medium pumping in the above-mentioned lasers was carried out by e-beam-controlled electric discharge. For the first time, such lasers were developed at the Physical Institute of the USSR Academy of Sciences³ and independently at the Los Alamos National Laboratory of the USA.⁴

In our country, they are known as electroionization lasers. Their creation became a significant milestone in the development of quantum electronics and opened a new avenue for construction of high-power and super-power laser systems.

In 1970–1980s, under the supervision of N.G. Basov, the high-power electroionization lasers have been developed for different technologies.^{5,6} Such lasers operated, as a rule, in a continuous mode, for which purpose heated electron emitters were used. The lasers could operate in a pulse-periodic mode as well. However, because of the limited emittance of the heated emitters, the peak radiation power increase was insignificant.⁷ At the same time, the pulse electronic accelerators with plasma emitters⁸ allowed an essential increase of the emitted current density.

In this paper, the main attention is given to the problem of construction of a reliable and high-power pulse-periodic CO₂ laser with a high energy in the pulse and controllable radiation duration for its application to various laser technologies.

1. The CO₂-laser design

The block diagram of the CO₂ electroionization laser is presented in Fig. 1. The basic units and elements of the laser are the gas-dynamic circuit 1,

fan 2, heat exchangers 3, 8, gas-discharge chamber 5, and electron accelerator 7.

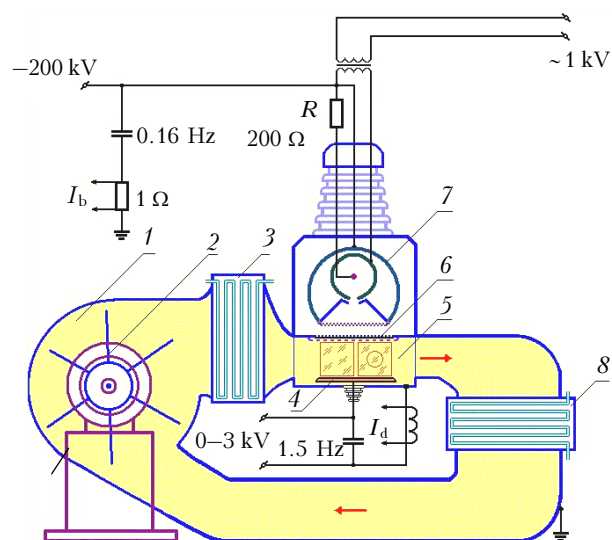


Fig. 1. Laser block diagram.

The volume of gas-dynamic circuit 1 is 3 m³. The circuit is pre-pumped up to 0.1 Torr. Then the volume is filled with a necessary amount of the gas mixture (nitrogen, helium, and carbon dioxide).

The gas flowing is performed by the diametrical fan 2 with an impeller of 580 mm in diameter and a blade of 720 mm in length.

The gas flowing speed at a working medium pressure of 50 Torr can be maintained at a level of 100 m/s.

The heat exchangers 3 and 8 are intended for cooling the working gas mixture. The heat exchanger 8 cools gas in the discharge chamber and regenerator, and the heat exchanger 3 cools the post-fan gas.

The gas-discharge chamber 5 consists of windows for gas stream input and output, a window for e-

beam input, a window for radiation output, as well as electrodes. The chamber is made of the stainless steel. The inner surface is lined with glass plates directing the gas stream and protecting chamber walls from the electric breakdown. The discharge area measures $10 \times 20 \times 100$ cm.

There is a foil unit 6 in the top of the discharge chamber, meant for separation of volumes of the accelerator 7 and the discharge chamber by the window, which is gas-tight and transparent for the e-beam. This unit consists of a cooled supporting lattice, on which the aluminum foil of $40 \mu\text{m}$ thickness is leaned by. On the discharge chamber side, an antistream lattice covers the foil protecting it from the electric discharge breakdown and serving as the top electrode of the discharge chamber.

In the discharge chamber bottom, anode 4 is located (active length of 100 cm and width of 20 cm), cooled by the running water. Bushings for anode feeding are made on the base of porcelain insulators.

The amplification factor M of the triple-pass telescopic resonator equals to 1.5. Mirrors are made of the oxygen-free copper. The radiation is output with the help of a rotating mirror through a KCl plate. The laser beam section has a form of a ring with an external and internal diameters of 100 and 60 mm, respectively.

The electron accelerator 7 serves to generate a ribbon e-beam with a section of 20×100 cm. It consists of the parallelepipedal case, lattice anode, and plasma cathode.

The case represents a stainless-steel welded construction (in the form of ribs) with windows for setting the foil unit, plasma cathode, and pumping collector of the high-vacuum system. A flange in the form of a plate with a sealed mouth is built-in to the case, to which the bushing isolator is connected. A constant voltage of 200 kV is applied to the diode cathode through the bushing isolator. Electrons, emitted by the plasma cathode, are accelerated in the diode gap between the plasma cathode and output window. A hermetic input with sylphon bellows and rotator, set on the bushing insulator, enables the cathode to be exposed relative to the output window of the foil unit.

In the described plasma cathode, the current of the glow discharge with a hollow cathode is closed to the anode through an extended slit. The current distribution along the slit, close to uniform, provides for generation of anode plasma, homogeneous in direction of the slit axis, and appearance of a plasma emitter with a large surface area.

The electrode system of plasma cathode (Fig. 2) includes a hollow cathode 1 of 200 mm in diameter and 1000 mm in length, as well as a hollow anode 2, a part of surface of which (180×1000 mm) is covered by the gauze screen 3. To initiate the discharge, the tungsten filament 4 stretched along the cathode axis, which is connected to the positive terminal of power source through the resistor R (see Fig. 1). The electrode system of the glow discharge is located inside the case 5 having the anode potential of the discharge.

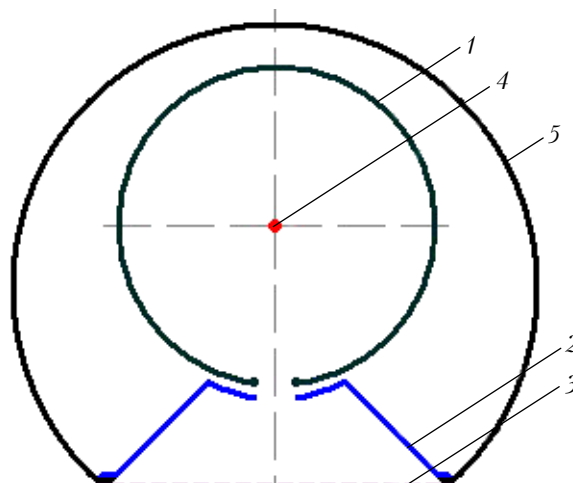


Fig. 2. Diagram of electrode system of plasma cathode: hollow cathode 1; hollow anode 2; gauze screen 3; initiating electrode 4; case 5.

The pulse e-beam generation at a constant accelerating voltage was provided by the pulse excitation of the glow discharge. The pulse voltage was applied to plasma cathode electrodes through the adapter transformer with insulation for a full operation voltage of the accelerator.

The working gas pressure (about 0.08 Pa) in the accelerator vacuum chamber (a width of the cathode aperture of 20 mm, air as the working gas) was determined by the combustion conditions of the glow discharge with a voltage of no more than 800 V.

2. Power characteristics of the CO₂ laser

Power characteristics of the CO₂ lasers depend on many initial parameters, such as discharge current, electric field intensity, composition and pressure of active medium, geometry of the active zone, etc. Therefore, no wonder that optimal generation conditions in different lasers differ.⁹ This necessitates carrying out of experiments on optimization of initial parameters of each new non-standard laser. Since the influence of the above-mentioned parameters on laser power has been investigated well enough,⁹ we briefly dwell on the experimental results on finding optimal generation conditions for the laser of interest.

2.1. Optimization of the gas mixture composition

In our experiments, the gas mixture pressure ($p = 50$ Torr), beam current density ($j_e = 0.05$ A/cm²), and the ratio of the field intensity to pressure ($E/p = 6$ V/(cm · Torr)) were maintained constant. When varying the proportion between CO₂ and N₂ in the absence of other components in the active volume, the maximal efficiency $\eta = 7\%$ was realized for CO₂ : N₂ = 1 : 9. Replacement of a part of molecular components by He led to the efficiency increase with

a maximum of 18% at $\text{CO}_2:\text{N}_2:\text{He} = 1:9:10$. A further increase of the He content in the gas mixture resulted in the efficiency decrease. The reason of such efficiency behavior is well-known and connected with the population decrease of the lower laser level 00^0_1 through the state 01^1_0 , which is most efficient at He ~ 50% in the active mixture.

At the same time, the maximal pulse power and energy are realized at $\text{CO}_2:\text{N}_2:\text{He} = 1:9:15$ due to increase of discharge power. A decrease of the molecular component content in the gas mixture leads to decrease of the ionization rate, which, however, is compensated by a decrease in the adherence rate. Therefore, the growth of current and discharge capacity, in our opinion, is connected with the increased electron drift velocity in the mixture with a higher He concentration at constant E/p .¹⁰

A further increase in the radiation energy may be at a sacrifice of partial replacing¹¹ of He by Ar having a greater section of ionization by electrons, that increases the discharge current density. Total replacing of He by Ar results in a decrease in radiation power and laser efficiency up to 8%. The best results are realized at $\text{CO}_2:\text{N}_2:\text{He}:\text{Ar} = 1:9:6:4$, i.e., through partial replacing of He by Ar in $\text{CO}_2:\text{N}_2:\text{He} = 1:9:10$, that allows increasing the radiation power by 25%. However, in this case, the efficiency falls from 18 to 16%.

2.2. Influence of field intensity in the interelectrode gap on the CO₂-laser radiation

An advantage of the active medium pumping by the e-beam-controlled semi-self-maintained discharge, is the opportunity of selection of such value for E/p , at which the main energy fraction enters the upper laser level.

The experiments with use of the $\text{CO}_2:\text{N}_2:\text{He} = 1:9:10$ mixture were carried out by two methods.

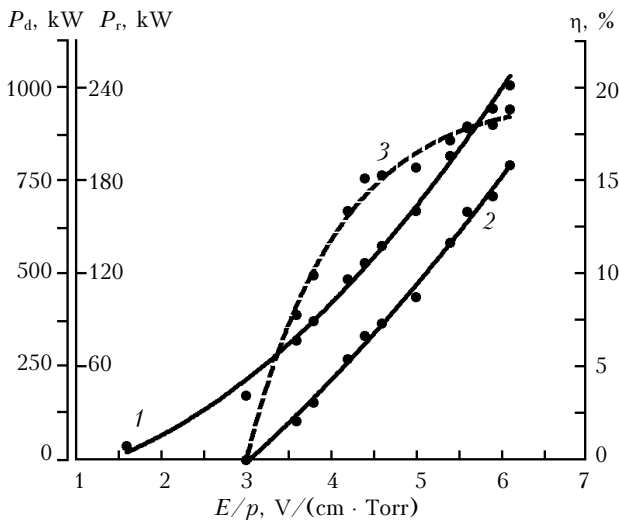


Fig. 3. Dependence of the discharge power P_d (1), radiation power P_r (2), and efficiency (3) on E/p .

In the first case, the gas mixture pressure varied at a constant voltage of the interelectrode gap; in the second case, the voltage increased at a constant pressure of

50 Torr. In both cases, the values of E/p were limited at a level of $6 \text{ V}/(\text{cm} \cdot \text{Torr})$ since a further increase led to the interelectrode gap breakdowns.

Figure 3 presents the dependence of discharge power (1), radiation power (2), and the efficiency (3) on E/p at $p = \text{const}$. As the field intensity increases a linear growth of both the discharge and radiation powers is observed, while the efficiency growth at an excess of $E/p = 4.5 \text{ V}/(\text{cm} \cdot \text{Torr})$ slows down. The lasing threshold at $\text{CO}_2:\text{N}_2:\text{He} = 1:9:10$ with a pressure of 50 Torr is observed at a field intensity of $150 \text{ V}/\text{cm}$.

2.3. Dependence of power characteristics on the e-beam current

Figure 4a presents oscillograms of the radiation pulse, discharge current, and electron beam current. It is seen that the electron beam magnitude determines the discharge current length, which, in turn, determines the radiation pulse length. As the e-beam length increased from 300 up to 1200 μs , the amplitude, rising edge and drop in pulses of the beam current, discharge current, and radiation remained invariable; the flat part length increased.

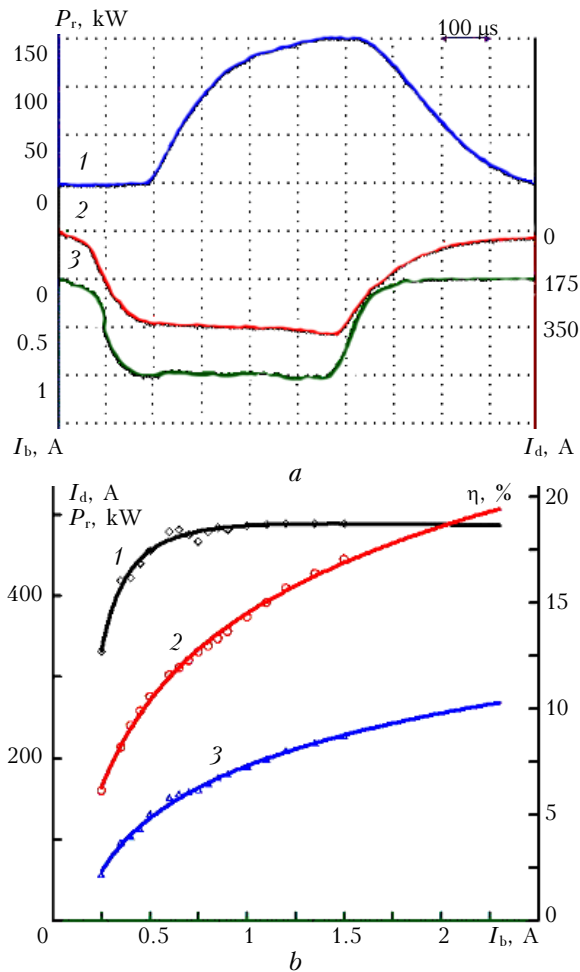


Fig. 4. Oscillograms of radiation pulse (1), discharge current (2), and e-beam current (3) (a); dependence of efficiency (1), discharge current I_d (2), and radiation power P_r (3) on e-beam current I_b (b).

Figure 4*b* shows the dependences of the efficiency, current discharge and radiation power on the e-beam current amplitude. The CO₂:N₂:He = 1:9:10 mixture pressure was 50 Torr; the interelectrode gap voltage was 2.8 kV. It is seen that at the beam current higher 0.5 A, the efficiency achieves its maximum of 18%; at the same values of the beam current, a slowing down of the discharge current and radiation capacity was observed.

Thus, in the course of the experiments, the starting conditions allowing one to achieve the maximal efficiency and radiation power were found.

3. Studies of the laser radiation focal spot

It is known that in pulse lasers of great volume, even insignificant heterogeneities of energy release in the active medium can lead to essential increase in the focal spot diameter. In particular, it was shown¹² that in the CO₂ laser with a working volume of 20 l at the atmospheric pressure in the mixture and a pumping time of 10 μs, within 3 μs there is no radiation whatsoever in the focal spot of the diffraction size because of the scattering.

In this work, we numerically and experimentally investigated the influence of pumping duration (energy) and heterogeneity in the gas pumping rate on the focal spot sizes.

3.1. The focal spot dynamics in the course of generation

At first, we investigated theoretically and experimentally the focal spot behavior in the course of generation.

At the first stage of computations, we solved the system of hydrodynamic equations for space distribution of the gas medium density and then, using the obtained results, we computed the changes in the medium optical properties. With the help of the Fresnel–Kirchhoff integral, the distortions of the electromagnetic wave distribution front were calculated. The characteristic curves of the gas density distribution in space are presented in Fig. 5.

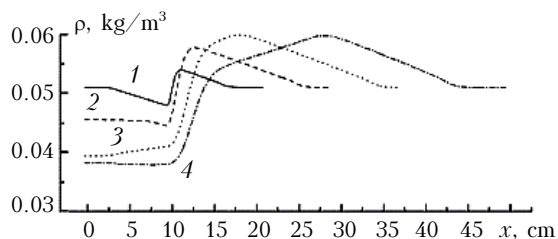


Fig. 5. Density distribution of gas medium in different moments: 250 (1); 500 (2); 750 (3); 1000 μs (4).

It is seen that a rarefaction wave directed inside the heating area and a compression wave directed outside are formed. Approximately for 500 μs, the rarefaction covers the entire heating area, and the

compression wave amplitude achieves its maximum. Further, the compression wave propagates from the heating area into the unperturbed medium, the rarefaction area being almost unchanged.

However, further computations of the Fresnel–Kirchhoff integral have shown that even most significant hydrodynamic distortions of the medium for the above-mentioned conditions do not exert essential influence on the electromagnetic field intensity distribution in the focal spot.

This conclusion has been proved experimentally.

The focal spot dynamics was investigated using radiation pulse imprints. The pulse was focused to the vinyl disk rotating at a revolution frequency ν of 11000 rpm. To reduce the target damage and the role of edge effects, the experiments were carried out with the focal spot of a sufficiently great size (~ 1.5 mm) and at decreased radiation powers ($P_r = 48$ kW).

Figure 6 demonstrates the results of radiation acting on a fixed plastic target and a rotating vinyl disk, as well as oscillograms of the radiation pulse corresponding to the moment of its acting on the vinyl target. It is seen, that at first, the width of the trace increases and by the end of the pulse decreases with decreasing radiation power. Any sharp changes in the trace width in the course of generation are not observed.

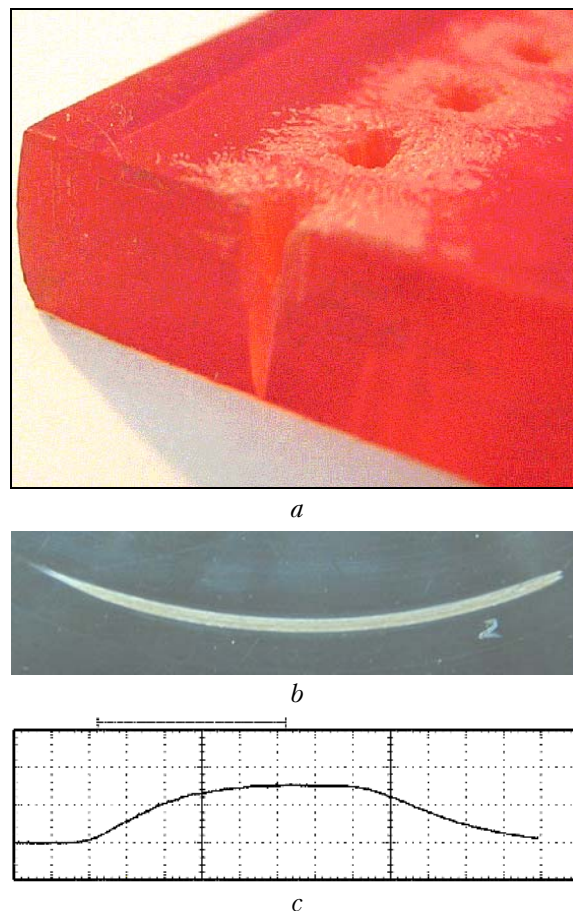


Fig. 6. Radiation trace on the fixed (a) and rotating (b) targets; oscillogram of the radiation pulse (c).

The experiments were carried out at pumping durations between 300 and 1200 μs . In all cases, the trace imprints are similar to that in Fig. 6*b*, only the trace length varied.

Thus, the computation and experiment have shown that when using the triple-pass telescopic resonator, the focal spot diameter does not increase despite the existence of zones with various gas temperatures.

3.2. Influence of heterogeneities in flowing on the radiation focal spot

It has been studied in the course of the experiments how considerably the heterogeneities in the gas flowing velocity can influence on the focal spot diameter.

In devices of such a class, the gas flowing velocity usually is about 100 m/s, and the inhomogeneities do not exceed 10%, that gives a difference in particle velocities in the stream section less than 10 m/s. Generation and estimation of inhomogeneities with such difference in stream velocities is a difficult problem to realize. Therefore, during the experiments, a half of the discharge zone was blown through at a velocity of 10 m/s, and in the other half, the gas stream was intercepted by a partition.

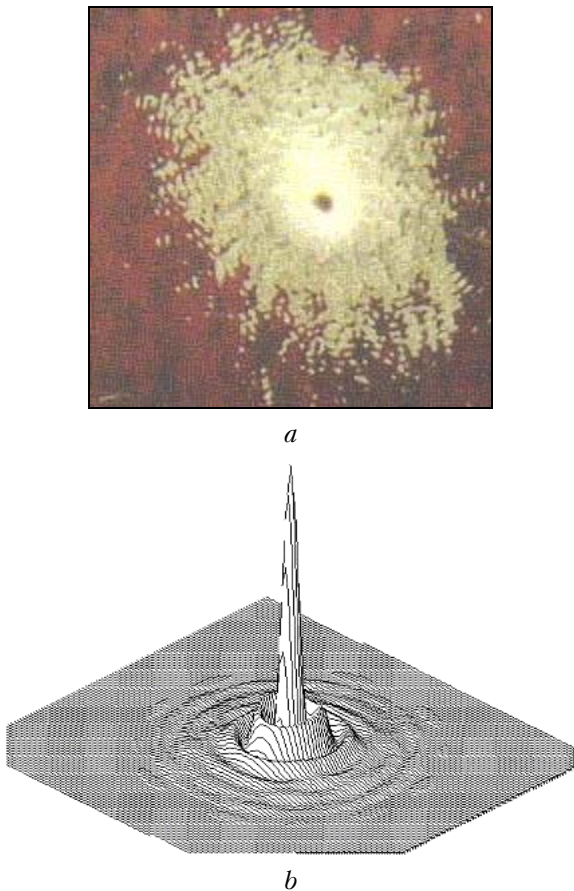


Fig. 7. The radiation trace on the target (*a*); the computed intensity distribution on the focal spot at the homogeneous gas flowing (*b*).

The imprints of the radiation focal spots on the plastic were recorded under conditions of the homogeneous gas stream (the discharge zone as a whole was blown) and the inhomogeneous one when the gas stream was partitioned (only a half of the discharge zone was blown). The photos of both imprints are presented in Figs. 7*a* and 8*a*.

It is seen, that the trace imprints differ. On inhomogeneous blowing, a portion of radiation moves upwards normally to the gas stream and aside opposite to the stream, almost 1.4 times increasing the focal spot in this direction (Fig. 8*a*).

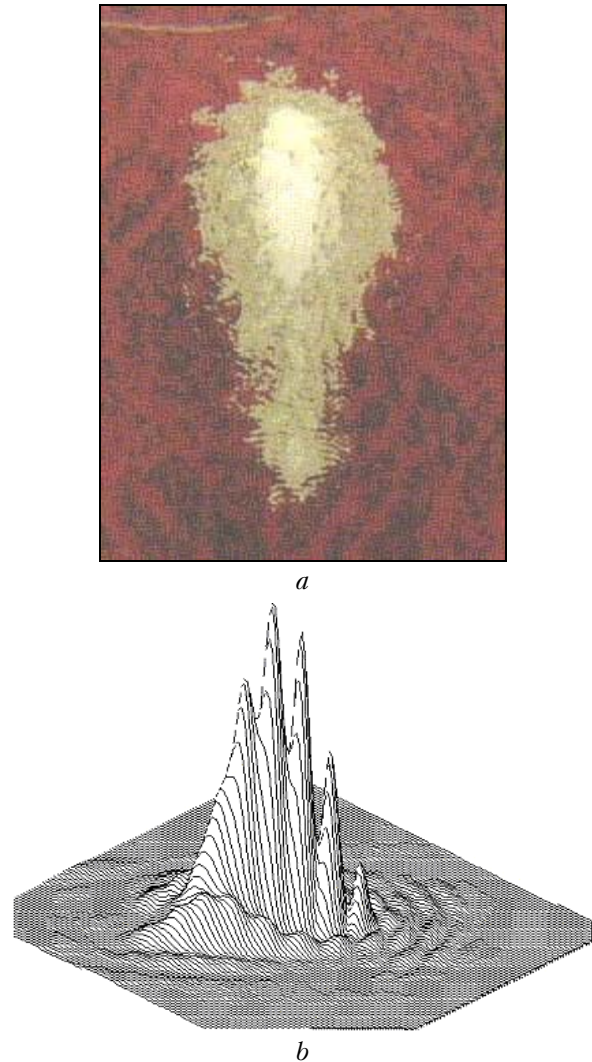


Fig. 8. Radiation trace on the target (*a*); theoretical computation of the intensity distribution in the focal spot at the heterogeneous gas flowing (*b*).

Note that when tuning the resonator additionally, the focal spot took its initial form (Fig. 7*a*). It is also interesting that if at this tuning the partition was removed and the gas stream became homogeneous, the focal spot trace had distortions opposite to those, which are presented in Fig. 8*a*. A further additional tuning of the resonator again returned the initial form and size to the focal spot, i.e., the effect had a reversible nature.

Under the impact of the pumping pulse of 700 μs length, the active medium is shifted by 0.7 cm lengthwise the gas stream, and as a result, about 7% of its volume is occupied by two zones with different radiation refractive indices.

This difference in homogeneity of the active medium, arising from blowing of the entire (Fig. 7*b*) or a part (Fig. 8*b*) of the interelectrode gap, was taken into account at focal spot computations. Comparison of computation results with the experimental data (Figs. 7*a* and 8*a*) shows their good qualitative and quantitative agreement.

Thus, the active gas medium heterogeneity causes a noticeable distortion of the wave front and, as consequence, of the radiation focal spot.

Conclusion

The CO₂ laser with plasma electron emitter in the system of the discharge preionization is characterized by high energetic parameters and has rather high radiation quality. These properties give the basis to consider the lasers prospective for industrial application.

References

1. B.M. Kovalchuk, V.V. Kremnev, and G.A. Mesyats, Dokl. Ros. Akad. Nauk **191**, No. 1, 76–78 (1970).
2. C.K.N. Patel, Phys. Rev. Lett. **13**, No. 21, 617–619 (1964).
3. N.G. Basov, E.M. Belenov, V.A. Danilychev, et al., Pis'ma Zh. Eksp. Teor. Fiz. **14**, Issue 7, 421–426 (1971).
4. C.A. Fenstermacher, M.J. Nutton, K. Boyer, and I.P. Rink, Bull. Phys. Soc. **16**, No. 4, 42–45 (1971).
5. A.P. Averin, N.G. Basov, L.A. Vasilyev, E.P. Glotov, M.I. Golovin, V.A. Danilychev, O.M. Kerimov, M.M. Malysh, V.M. Semerov, A.M. Soroka, N.D. Ustinov, N.V. Cheburkin, and V.I. Yugov, Sov. J. Quant. Electron. **12**, No. 12, 1537–1538 (1982).
6. A.P. Averin, N.G. Basov, E.P. Glotov, V.A. Danilychev, L.N. Drachuk, O.M. Kerimov, I.N. Matveev, A.M. Soroka, A.M. Sornik, N.D. Ustinov, N.V. Cheburkin, and V.I. Yugov, Sov. J. Quant. Electron. **13**, No. 10, 1391–1393 (1983).
7. N.G. Basov, V.V. Bachenko, E.P. Glotov, S.G. Gornyi, V.A. Danilychev, G.N. Karpov, V.A. Lapota, M.M. Malysh, N.G. Rudoi, V.A. Saburov, and A.M. Soroka, Izv. Vyssh. Uchebn. Zaved., Ser. Fiz. **48**, No. 12, 2310–2320 (1984).
8. S.P. Bugaev, J.E. Kreindel, and P.M. Shchanin, *E-beams of Large Section* (Energoatomizdat, Moscow, 1984), 112 pp.
9. G.A. Mesyats, V.V. Osipov, and V.F. Tarasenko, *Pulsed Gas Lasers* (Nauka, Moscow, 1991), 272 pp.
10. A.N. Lobanov and A.F. Suchkov, Sov. J. Quant. Electron. **4**, No. 7, 843–848 (1974).
11. A.P. Averin, N.G. Basov, E.P. Glotov, V.A. Danilychev, N.N. Sazhina, A.M. Soroka, and V.I. Yugov, Sov. J. Quant. Electron. **11**, No. 9, 1260–1262 (1981).
12. D.R. Suhre, M.J. Pechersky, J.F. Lowry, and J.F. Roach, J. Appl. Phys. **65**, No. 3, 954–958 (1989).